Mechanical enhancement and weakening in Mo_6S_6 nanowire by twisting

Ke Xu(徐克)[1], Yanwen Lin(林演文)[1], Qiao Shi(石桥)[1], Yuequn Fu(付越群)[1], Yi Yang(杨毅)[2], Zhisen Zhang(张志森)[1,†], and Jianyang Wu(吴建洋)[1,3,‡]

[1] *Department of Physics, Research Institute for Biomimetics and Soft Matter, Jiujiang Research Institute and Fujian Provincial Key Laboratory for Soft Functional Materials Research, Xiamen University, Xiamen* 361005, *China*

[2] *Jiangsu Key Laboratory of Advanced Food Manufacturing Equipment and Technology, Jiangnan University, Wuxi* 214122, *China*

[3] *NTNU Nanomechanical Laboratory, Norwegian University of Science and Technology, Trondheim* 7491, *Norway*

(Received 8 August 2022; revised manuscript received 8 November 2022; accepted manuscript online 2 December 2022)

The torsional, bending and tensile mechanical properties of Mo_6S_6 nanowire are examined by molecular dynamics (MD) simulations with a first-principles-based reactive force field (ReaxFF). It is found that Mo_6S_6 nanowire shows unique mechanical properties such as high torsional and bending flexibility, high Young's modulus and strength, and negative Poisson's ratio. The Mo_6S_6 nanowire can be strengthened or weakened via twisting, depending on the twist angle. The Mo_6S_6 nanowire with a slight twist angle shows brittle failure, whereas it with a large twist angle exhibits ductile failure and necking behavior. Twisted Mo_6S_6 nanowires show a crossover in the negative Poisson's ratio at critical strains, that is, Poisson's ratio first decreases but then increases, with a minimum value down to around -0.8 at the strain of 0.01 as the twist angle is 21.0 °/nm. The negative Poisson's ratio and the crossover are explained by the bond transform that makes zero angles to the wire cross-section.

Keywords: Mo_6S_6 nanowire, mechanical properties, twisting, negative Poisson's ratio

PACS: 62.20.M–, 62.20.dj, 62.23.Hj, 02.70.Pt **DOI:** 10.1088/1674-1056/aca7e7

1. Introduction

From fundamental science and technological application points of view, low-dimensional materials have attracted much interest because they exhibit a kaleidoscope of fascinating properties. For example, two-dimensional (2D) graphene and one-dimensional (1D) carbon nanotubes (CNTs) are reported to show extremely high tensile strength,[1] high Young's modulus and high thermal conductivity,[2] as well as large carrier mobility.[3] Thereby, they find important applications in microelectromechanical systems (MEMS) and nanoelectromechanical systems (NEMS) devices.[4,5] Besides, 1D silicon nanotube[6] and 1D diamond nanowires[7] also show unique mechanical and thermal properties, and the elastic modulus of linear carbyne crystals can be near the predicted bounds.[8–10]

Recently, Mo_6S_6 nanowire (NW), as a new class of transition metal chalcogenide (TMC) NWs, has been fabricated under diverse experimental settings. For example, using the Cu (111) surface, the growth of Mo_6S_6 NWs aligned with the substrate directions was identified.[11] Via an e–beam irradiation process combined with high temperature heating, Mo_6S_6 NWs were formed in the edges of monolayer molybdenum disulfide (MoS_2).[12] The properties of Mo_6S_6 NW were also reported. For example, due to the hydrodynamics efforts, Mo_6S_6 NW possesses high thermal conductivity.[13] Because of its strong hybridization between Mo d-orbitals and S p-orbitals, Mo_6S_6 NW shows uniaxial metallic characteristics,[14] and its conductivity is better than CNTs.[15] Subjected to torsional and bending deformations, Mo_6S_6 NW remains conductive.[16] Mechanically, it was via first-principles calculations reported that Mo_6S_6 NW shows good tensile properties, for example, with Young's modulus and maximum tensile strength of around 300 GPa and 19 GPa,[17–19] respectively. Using classic molecular dynamics (MD) simulations, it was found that Mo_6S_6 NW has Young's modulus, fracture strength and fracture strain of around 300 GPa, 56.4 GPa, and 0.29 GPa,[20] respectively. Under uniaxial loading, a novel phase transformation was observed in Mo_6S_6 NW. Furthermore, Mo_6S_6 NWs can be used to manipulate the electronic properties of the nanowires by iodine doping.[21] Intriguingly, as it is critically twisted, the transition of metal-to-semiconductor of Mo_6S_6 NW occurs.[19,22,23] As a result, Mo_6S_6 NW can be utilized as cables to flexibly transfer information between electromechanical switches through strain engineering and can be used as novel building blocks for future nanodevices.

As a nanoscale electromechanical switch, the mechanical characteristics of Mo_6S_6 NW are of critical importance. However, they remain largely unknown, particularly when it is twisted. In the present study, the tensile and bending properties of twisted Mo_6S_6 NW are comprehensively investigated using the first-principles-based ReaxFF MD simulations. This study provides new insights into the mechanics of 1D Mo_6S_6 NW, which contributes to its promising applications.

†Corresponding author. E-mail: zhangzs@xmu.edu.cn

‡Corresponding author. E-mail: jianyang@xmu.edu.cn

© 2023 Chinese Physical Society and IOP Publishing Ltd

2. Model and methods

2.1. Atomic model of Mo_6S_6 nanowire

Figures 1(a)–1(d) show the atomic structure of twist-free Mo_6S_6 NW from three aspects, which is constructed on the basis of experimental characterization data.[16] As shown in Figs. 1(a) and 1(b), one unit-cell of Mo_6S_6 NW comprises two layers. The two layers of atoms are mismatched by 60° in the axial direction. Each layer is composed of 3Mo + 3S atoms, where Mo and S atoms are located in the inner and outer regions of axial wire, respectively, as shown in Figs. 1(c) and 1(d). Each elemental atom has 4 neighbors with the other elemental atom, with 2 and 2 on the vertical and parallel axis, respectively. The 6 Mo atoms in the staggered atomic triangles structurally form an octahedron, as shown in Fig. 1(d). In this study, twisted Mo_6S_6 NWs are generated by twisting the wire along the axis, as illustrated in Fig. 1(b). The twist angle is defined as $\alpha = \theta/L$, where θ and L are the twisted angle and the axial length of a specific length of wire, respectively. In order to achieve a wide range of α, Mo_6S_6 NW with 25 unit-cells is generated to achieve torsional deformation. Here, 7 twisted Mo_6S_6 NWs with $\alpha = 10.5$ °/nm, 21.0 °/nm, 31.7 °/nm, 42.4 °/nm, 53.3 °/nm, 64.2 °/nm, and 75.2 °/nm are generated. Figures 1(e) and 1(f) display the top-views of Mo_6S_6 NW with $\alpha = 10.5$ °/nm and 31.7 °/nm, while figures 1(g) and 1(h) show the perspective view of Mo_6S_6 NW with $\alpha = 0$ °/nm and 31.7 °/nm.

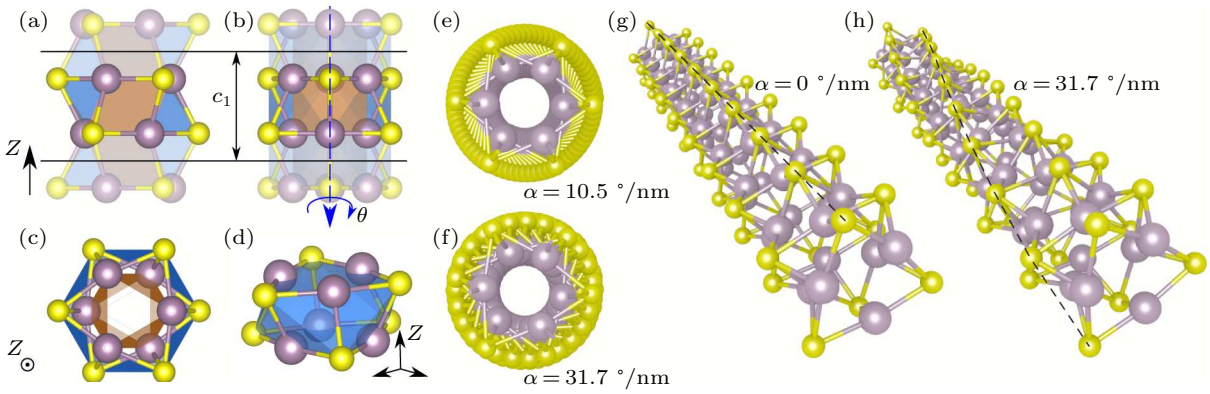


Fig. 1. Schematic diagram of the structure of the Mo_6S_6 NWs. (a)–(c) Three primary orthographic views of the Mo_6S_6 nanowire, which are front, side, and top views, respectively, in which the orange and blue polyhedrons are used to represent the octahedron composed of central Mo atoms and outer edge S atoms, respectively. Panel (d) is the free perspective. Panels (e) and (f) are the top views of the torsion models with $\alpha = 10.5$ °/nm and 31.7 °/nm, respectively. Panels (g) and (h) are the perspective of a representative twisted Mo_6S_6 NWs of model with $\alpha = 0$ °/nm and 31.7 °/nm.

2.2. MD simulations

Initially, structural optimization and relaxation are performed to obtain stable configurations of twist-free and twisted Mo_6S_6 NWs. In the structural optimization, all studied Mo_6S_6 samples are quasi-statically optimized to a local energy-favorable configuration by the conjugate gradient method, in which the energy and force tolerances are assigned to be 10^{-5} kcal/mol and 10^{-5} kcal/(mol·Å), respectively. In the structural relaxation, MD calculations with a simulation time of 1 ns are carried out at a given temperature and pressure of 0 under the NPT (constant number of particles, constant pressure and constant temperature) ensemble. Afterward, as-relaxed Mo_6S_6 NWs are uniaxially stretched with a constant engineering straining rate of 10^7 s^{-1} to examine their mechanical properties. During the uniaxial stretching, the temperature and pressure in the transverse directions are controlled by the Nosé–Hoover thermostat and Nosé–Hoover barostat methods with damping times of 100 timesteps and 1000 timesteps, respectively. The velocity-Verlet integration method with a timestep of 0.2 fs is adopted to integrate Newton's motion in the Mo_6S_6 NW system. The global tensile stresses (σ) are computed as follows:

$$\sigma = \frac{Nk_BT}{V} + \frac{\sum_i^{N'} \boldsymbol{r}_i \cdot \boldsymbol{f}_i}{dV}, \tag{1}$$

where N, T, and V are the number of atoms, temperature, and volume of the systems. k_B is Boltzmann's constant. $\boldsymbol{r}_i$ and $\boldsymbol{f}_i$ are the position and force of atom i, respectively. Here, the diameter of Mo_6S_6 NW is chosen as 0.6 nm.[24]

All the simulations are realized via the Large-scale Atomic/Molecular Massively Parallel Simulator (LAMMPS) open-source code.[25,26] The first-principles-based ReaxFF potential[27] is used to describe the atomic interactions in both twist-free and twisted Mo_6S_6 NWs. Chemical behaviors such as dissociation and reformation of covalent bonds during MD simulations can be described by the ReaxFF force field because it includes bond order-dependent covalent interactions and non-bonded Coulomb and Morse interactions. To date, it has shown that the chemical, mechanical and thermal behaviors of various Mo–S nanostructures can be predicted by the ReaxFF forcefield.[13,28–30] In this work, the ReaxFF forcefield developed by Alireza *et al.*[28] is employed to investigate the mechanical characteristics of Mo_6S_6 NWs.

3. Results and discussion

This section is mainly divided into four subsections to introduce the mechanical properties of Mo_6S_6 NW. Firstly, the structural properties such as lattice constant and structural stability of Mo_6S_6 nanowire are displayed and the corresponding discussion are made. Next, the torsional and bending properties are then discussed separately to derive their torsional stiffness in bending stiffness. Then, the axial tensile behaviors of twist-free and twisted Mo_6S_6 nanowire are displayed, in terms of mechanical properties such as strength, modulus, fracture mechanisms. Finally, the anomalous Poisson's ratio of Mo_6S_6 NW is studied and analyzed.

3.1. Lattice constant and structural stability

In this study, the axial length of the unit-cell of twist-free Mo_6S_6 NW (lattice constant) is predicted to be around 4.6 Å, which is slightly larger than the experimental data (4.5 + 0.005 Å)[14] and the first-principles calculations (4.4 Å).[16] This indicates that the ReaxFF potential used in this study can appropriately describe the atomic interactions in the Mo_6S_6 NW system. Figure 2(a) shows the ratio of the lattice constant of twisted-to-twist free Mo_6S_6 NW as a function of α. As can be seen, the normalized lattice constant of Mo_6S_6 NW is almost linearly reduced with increasing α. This indicates that Mo_6S_6 NW is axially shortened as it is twisted, originating from the Poisson effect. From Fig. 2(a), it deduces that the axial length (L_z) and α of Mo_6S_6 NW follow a linear function of $L_z = 115.07 - 0.0469\alpha$.

The thermal stability of Mo_6S_6 NW subjected to torsional deformations is also investigated. Figure 2(b) shows the upper-bound temperature tolerance (T_u) of Mo_6S_6 NW as a function of α. Here, the T_u is defined as above which bond dissociation occurs, accompanied by a sudden drop in the potential energy (E_p). Apparently, the T_u of Mo_6S_6 NW is monotonically reduced with increasing α. However, there is a critical angle range with intermediate value $\alpha \simeq 31.7$ °/nm for the T_u of Mo_6S_6 NW. Below this, a linear function of $T_u = -3.2\alpha + 1915$ can be fitted, whereas above which, $T_u = -15.5\alpha + 2300$, the reduction in the T_u becomes more pronounced.

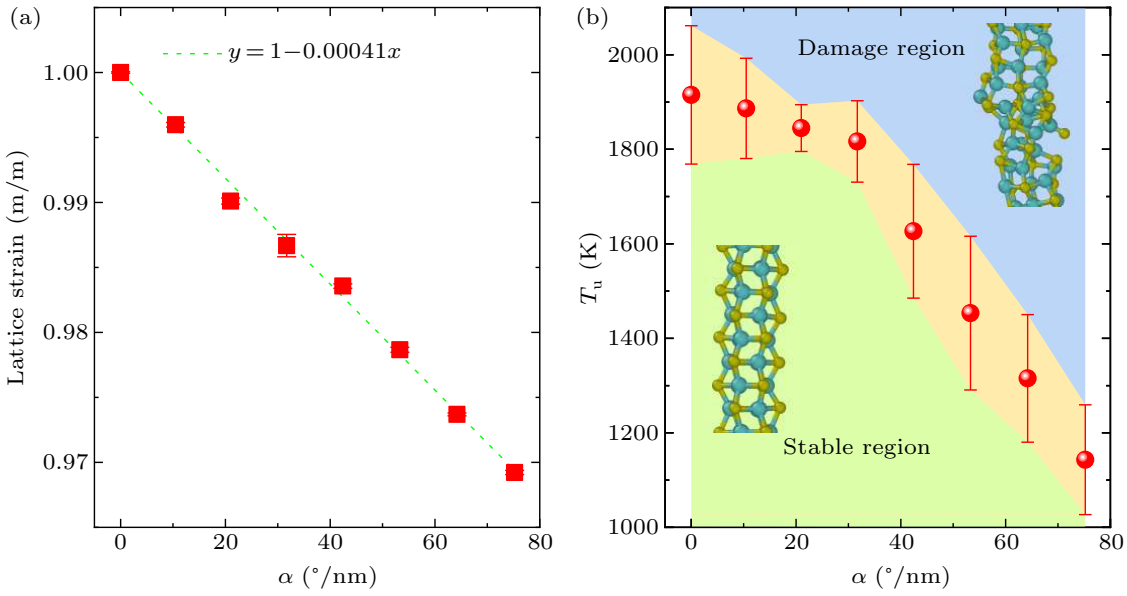


Fig. 2. (a) The relationship between the torsion angle α and lattice strain. (b) High-temperature tolerance of Mo_6S_6 nanowire. The green/blue region represents the low-temperature stable/damage.

3.2. Twist and bending stiffness

Figure 3 shows the variation in the difference of the ΔE_p between twisted and twist-free Mo_6S_6 NW with α (Fig. 3(a)) and θ (Fig. 3(b)). Here, the ΔE_p is defined as $E - E_\alpha$, where E, E_α are the energies of the Mo_6S_6 NW system when α is equal to 0 and other finite values, respectively. It is observed that the ΔE_p becomes more pronounced with increasing α. From an elastic mechanics point of view, when a rod body is elastically twisted around the longitudinal axis of the rod, the torsional stiffness (k) of a wire can be computed as follows:[31]

$$k = \frac{N}{L}\frac{\partial^2 E_s}{\partial \theta^2}, \tag{2}$$

where L and N are the length and the atom number of the wire, respectively. E_s is the normalized elastic energy per atom. $\theta = \alpha L$ is the applied torsional angle in the wire. Using the data of Fig. 3(a), the k of Mo_6S_6 NW is determined to be around 3.26×10^{-4} kcal/mol/nm/deg^2. Table 1 lists the k of Mo_6S_6 NW, as well as other 1D nanostructures. By comparison, the k of Mo_6S_6 NW is found to be 2 orders of magnitude lower than that of (5,5) and (10,10) CNTs,[32] but 3 orders of magnitude lower than that of Si NW,[33] indicating its superhigh torsional flexibility.

For a value of bending angle (β), the loading curve is quadratic and the bending stiffness (D) as defined in Ref. [31]

is determined as follows:

$$D = \frac{N}{L}\frac{\partial^2 E_s}{\partial \beta^2}, \tag{3}$$

where β is the function of the radius (R) of Mo_6S_6 NW. With regard to the calculation of the D, Mo_6S_6 NW with different L_z is uniquely deformed into ring-like structures. Figure 4(a) plots the difference in the ΔU between the ring and bending-free Mo_6S_6 NW, ΔU subjected to various α as a function of the radius of Mo_6S_6 NW ring, as well as a representative ring structure obtained from Mo_6S_6 NW. Apparently, the ΔU greatly depends on the radius (R) of Mo_6S_6 NW, as well as the α. From an elastic mechanics point of view, the deformation energy (ΔU) of a uniform nanowire under pure bending load is expressed as follows:

$$\Delta U = \frac{1}{2} SDR^{-2}, \tag{4}$$

where S and R are the cross-sectional area and the radius of curvature of the nanowire, respectively. Using Eq. (4), the D of silicon core/shell nanowires is obtained.[33] Similarly, the D of Mo_6S_6 NW subjected to different α is also calculated on the basis of elastic mechanics. Here, the cross-sectional area of Mo_6S_6 NW (S) subjected to different α is given by $S = \pi r^2$, where $r = 0.3$ nm. The R is defined as follows:

$$R = \frac{1}{N}\sqrt{\sum_{m=x,y}\sum_{i=1}^{N}(m_i - m_c)^2}, \tag{5}$$

where $m_c = (1/N)\sum_{i=1}^{N} m_i$, N is the total number of atoms in the Mo_6S_6 ring NW. The NW radius R_{nt} is assumed to be the radius of curvature R. The D of Mo_6S_6 NW subjected to different α can be obtained by fitting the data in Fig. 4(a). Table 2 lists the D of twist-free Mo_6S_6 NW, as well as that of other low-dimensional materials.[34–39] By comparison, the D of Mo_6S_6 NW is found to be 1 order of magnitude lower than that of CNTs, but 2 orders of magnitude lower than that of MoS_2 nanotube (NT). Moreover, the D of Mo_6S_6 NW is even significantly lower than monolayer graphene,[36,37] monolayer black phosphorus[34] and monolayer MoS_2,[35] whose layer thicknesses are smaller than the radius of Mo_6S_6 NW. This indicates that Mo_6S_6 NW possesses high bending flexibility. Figure 4(b) shows the D of Mo_6S_6 NW as a function of α, in which the bond color code of the insets for the bonds is on the basis of the values of the bond length. It is observed that the D monotonically increases with increasing α, varying from 1.81 kcal/mol to 6.65 kcal/mol. This indicates that the D of Mo_6S_6 NW is effectively enhanced by twisting operations. It is, however, observed a critical α in the changing of the D of Mo_6S_6 NW. Below $\alpha \simeq 53.3$ °/nm, the increase in the D becomes significant with increasing α, whereas above which, the increase in the D becomes less significant with increasing α. The insets in Fig. 4(b) and Fig. S1 indicate that, as Mo_6S_6 NW is bent with different bending curvature, it shows distinct bond configurations.

Table 1. Comparison of torsional stiffness (k) of Mo_6S_6 NW with other 1D materials.

Structure	Torsion stiffness (k) (kcal/mol/nm/deg^2)	Refs.
Mo_6S_6 NW ($R = 0.3$ nm)	3.26×10^{-4}	this work
Si NW ($R = 2.1$nm)	2.35×10^{-1}	[33]
Single-walled CNT (5,5)	2.32×10^{-2}	[32]
Single-walled CNT (10,10)	4.71×10^{-2}	[32]

Table 2. Comparison of bending stiffness (D) of Mo_6S_6 NW with other low-dimensional materials.

Structure	Bending stiffness (D) (kcal/mol)	Refs.
CNT ($R = 0.44$ nm)	19.6	[38]
MoS_2 nanotube ($R = 1$ nm)	108–226	[39]
Graphene	27.7, 32.3	[36,37]
Single layer black phosphorus	28.8, 123.1	[34]
Single layer MoS_2	152.0–304.0	[35]
Mo_6S_6 NW ($R = 0.3$ nm)	1.81	this work

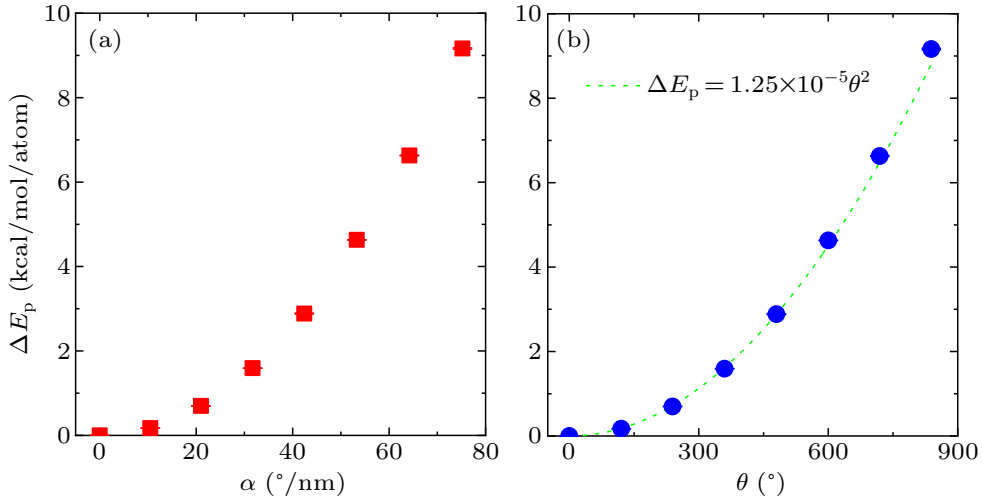


Fig. 3. The relationship between the torsion angle (a) α, (b) θ and torsional strain energy.

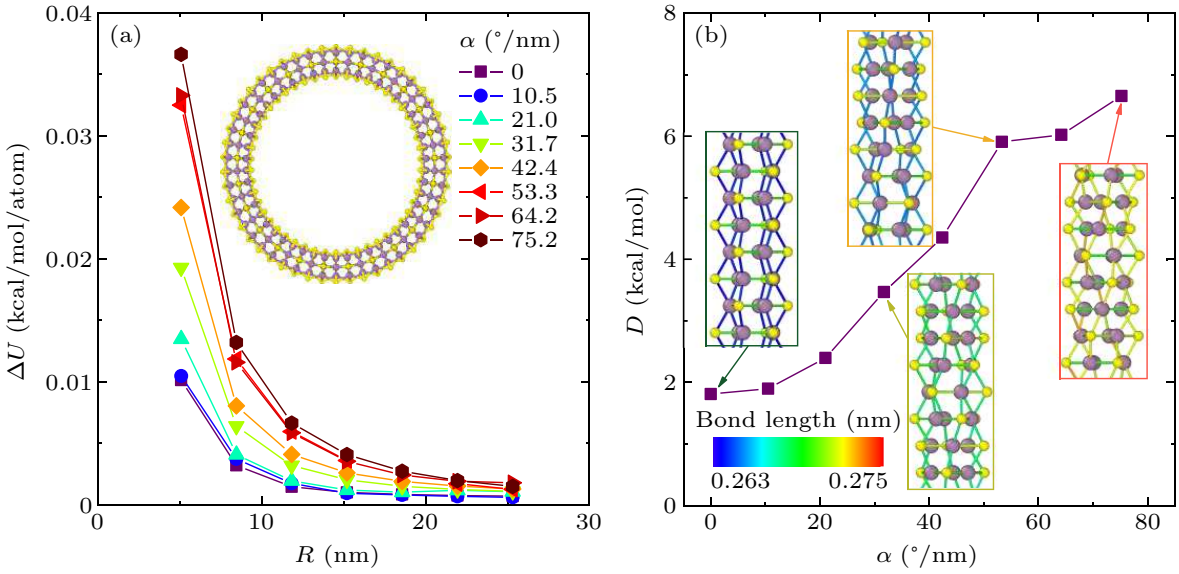


Fig. 4. (a) Bending energy as a function of the radius (R) of Mo_6S_6 ring NW. (b) D as a function of the α. The bond colors in the subgraph are colored by bond length.

3.3. Effects of twist on the loading response and deformation mechanism

Figures 5(a)–5(f) show the tensile stress–strain responses of Mo_6S_6 NWs subjected to different α. From the responses, three to five deformation stages can be identified, depending on the value of α. When $\alpha \leq 31.7$ °/nm, Mo_6S_6 NW shows three deformation stages, whereas 31.7 °/nm $< \alpha \leq 53.3$ °/nm and $\alpha > 53.3$ °/nm Mo_6S_6 NW exhibit four and five deformation stages, respectively. For all cases, the deformation stages I and II are characterized by linear and nonlinear stress–strain curves, during which it is elastically stretched. In the deformation stage II, the increase in the loading stress becomes significant with increasing axial strain, namely, the slope of the tensile stress–strain curves is monotonically enhanced with increasing strain. The deformation stage III of Mo_6S_6 NW with $\alpha \leq 53.3$ °/nm is mainly described by a sudden drop of loading stress to zero in the loading curves, signifying the axial tension failure of Mo_6S_6 NW. When $\alpha \leq 31.7$ °/nm, the loading stress remains zero with increasing strain, indicating their brittle separation. For Mo_6S_6 NW with $\alpha \geq 64.2$ °/nm, the deformation stage III is defined by the strain regime, which starts from the turning point at which the increase of the loading stress becomes less significant and terminates at the strain and the maximum loading stress is achieved. In this deformation stage, the turning point in the loading stress indicates the occurrence of structural transformation. Such structural transformation leads to a reduction of tensile stiffness. The deformation stage IV of Mo_6S_6 NW with 31.7 °/nm $< \alpha \leq 53.3$ °/nm is characterized by re-risings and drops of loading stress in the curves, indicating its large plastic deformations. The deformation stages IV and V of Mo_6S_6 NW with $\alpha \geq 64.2$ °/nm are similar to the deformation stages III and IV of Mo_6S_6 NW with 31.7 °/nm $< \alpha \leq 53.3$ °/nm, respectively.

Table 3. Comparison of Young's modulus of Mo_6S_6 NW with other 1D material.

Structure	Young's modulus (Y) (GPa)	Refs.
MoS_2 nanotube (20,20) 1 K	125	[45]
MoS_2 nanotube (35,0) 1 K	110	[45]
MoS_2 nanotube (8 nm)	230	[46]
CNT ($R = 0.4$ nm–2.0 nm)	890–1040	[41]
TiO_2 nanotube	23–44	[42]
WS_2 nanotube	150–170	[44]
MoS_2 nanotube	170–250	[35]
BN nanotube	850	[43]
Mo_6S_6 NW ($R = 0.3$ nm)	481	this work

As shown in Fig. 5(i), Mo_6S_6 NWs with eight different α show similar variation in the strength (σ_{max}) and strain (ε_b) with α. The gravimetric strength ($\sigma_{\rho-max}$) of those Mo_6S_6 NWs is listed in Table S1. It is revealed that as α increases, the σ_{max} or ε_b initially increases but then decreases, in which the crossover occurs at $\alpha = 21$ °/nm–32 °/nm. It is noted that the gravimetric Young's modulus (Y_ρ)[8–10,40] can be commonly utilized for mechanically characterizing low-dimensional materials to avoid controversies in the definition of cross-sectional area. Here, the Y_ρ is defined as the Y of a material (Y) divided by the original mass density (ρ): $Y_\rho = Y/\rho$. Figure 5(h) shows the Y and Y_ρ of Mo_6S_6 NW with eight different α. Interestingly, the variations in the Y and Y_ρ with α are different from those of the ultimate stress–strain. For example, with the increase of α, there is initial reduction tendency in the Y and Y_ρ but then an increase trend is identified. Table 3 shows the comparison of Y of typical 1D materials.[35,41–46] Apparently, it is seen that the twist-free Mo_6S_6 NW is very competitive to those mechanically robust 1D materials in terms of the Y. The gravimetric strain–stress curves of Mo_6S_6 NWs are shown in Fig. S2.

As can be seen, due to the heavy-weight chemical composition, the Y_ρ of Mo_6S_6 NW (62.5 GPa·g^{-1}·cm^3) is an order-of-magnitude smaller than that of carbynes@CNT composites (356.4 GPa·g^{-1}·cm^3–906.8 GPa·g^{-1}·cm^3)[9] as shown in theTable S2.

To further understand the deformational mechanisms underlying the loading responses, the developments of molecular configurations of twist-free and twisted Mo_6S_6 NW are recorded. As a representative, the snapshots of Mo_6S_6 NW with $\alpha = 0$ °/nm, 42.4 °/nm, and 64.2 °/nm at critical axial strains are displayed in Fig. 6, as well as their loading curves. Note that the color code in the snapshots is on the basis of the atomic shear strain. As shown in Fig. 6(b), the configuration is uniformly stretched during the deformation stages I and II. When the elongation is critically imposed, the configuration of Mo_6S_6 NW fails via brittle fracture. When 31.7 °/nm $< \alpha \leq$ 53.3 °/nm, the deformation mechanism is representatively illustrated in Fig. 6(e). Prior to a sudden drop of loading stress, it is uniformly elongated. As the axial stretching is critically applied, bond dissociations nucleate at a local region to release the strain energy. The releases of strain energy result in the following re-rising loading stress. Intriguingly, as a result of localized bond dissociation, necking occurs, similar to metallic NWs.[47] Subsequently, an atomic chain formed, which is also observed in stretched MoS_2 nanostructures[4,48–50] and stretched defective CNTs.[51–54] Finally, it completely fractures at a large strain. When $\alpha \geq 64.2$ °/nm, the deformation mechanism is illustrated in Fig. 6(f). As is indicated, there is a local structural transformation in the deformation stage III, while the deformation behavior is similar to the case in Mo_6S_6 NW with 31.7 °/nm $< \alpha \leq 53.3$ °/nm.

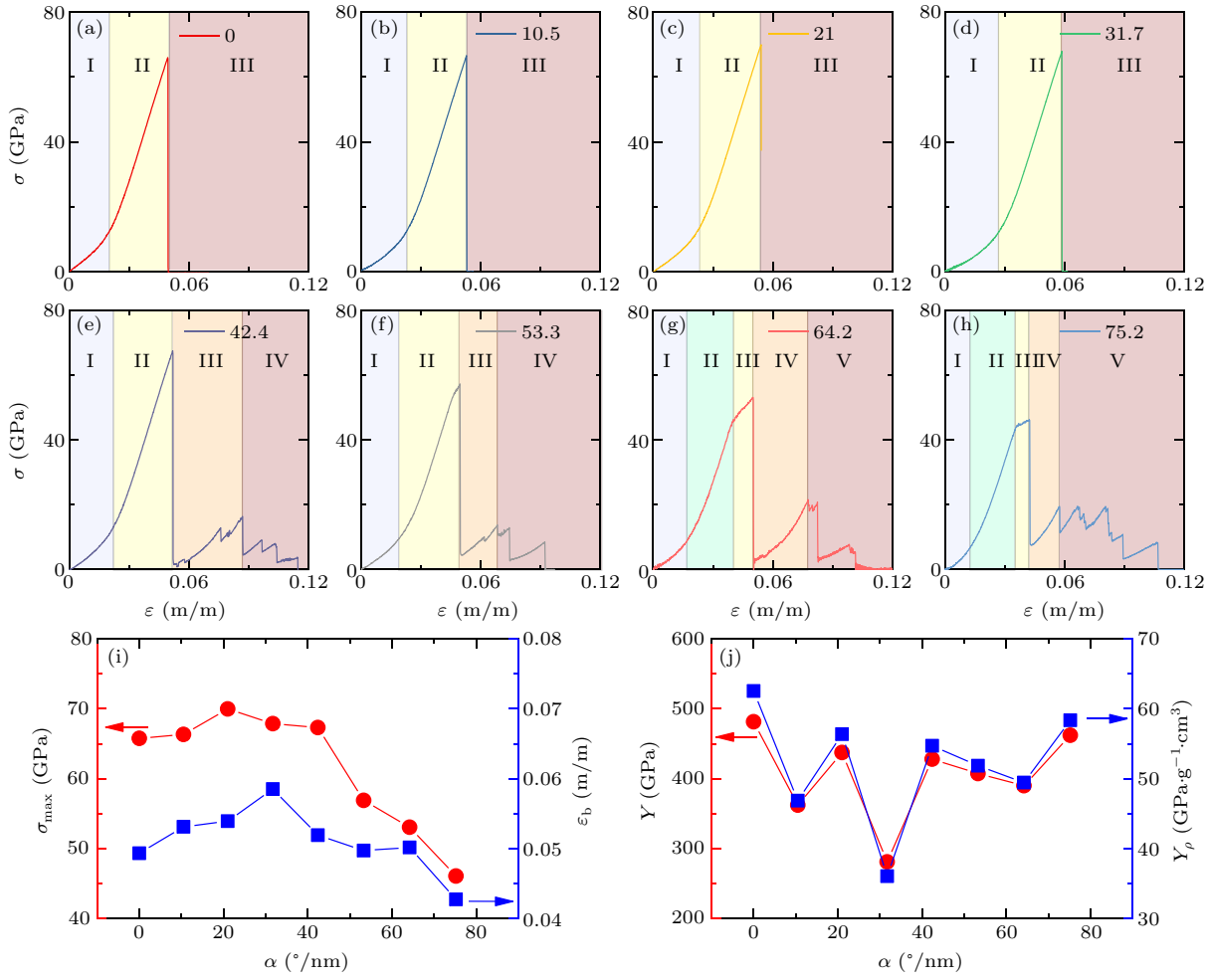


Fig. 5. (a)–(h) Mechanical stress–strain curves of eight Mo_6S_6 NW torsional models at 300 K. (i) The failure stress and strain of eight Mo_6S_6 NW torsional models. (j) The Y and gravimetric Y_ρ of eight Mo_6S_6 NW torsional models.

3.4. Negative Poisson's ratios

In mechanics, Poisson's ratio (μ) is also a common way to characterize the elastic properties of a material, and it is defined by the negative of the ratio of the contraction strain (transverse, lateral or radial strain, ε_t) to the loading strain (or axial strain, ε_l), with formula of $\mu = -\varepsilon_t/\varepsilon_l$. Figure 7 shows the variations in the Poisson's ratio (μ) of Mo_6S_6 NW with α. As shown in Fig. 6(a), all investigated Mo_6S_6 NWs yield apparent negative μ as they are elastically stretched. Intriguingly, it identifies a flipped behavior in the negative μ at critical strains. Below which, the μ value reduces with increasing strain, however, above which, the μ value is increased with

increasing strain. The flipped behavior indicates the transformation of bond configurations subjected to critical straining. However, the value of critical strain at which the flipped behavior depends on α. The minimum μ value can be down to around -0.8 for Mo_6S_6 NW when $\alpha = 21.0$ °/nm, suggesting strong auxetic behavior. To date, negative μ is identified in 2D materials,[55–57] as well as artificially designed nanostructures.[58,59] However, it is rarely observed in 1D materials with negative μ. This is one of the advanced mechanical properties of Mo_6S_6 NW.

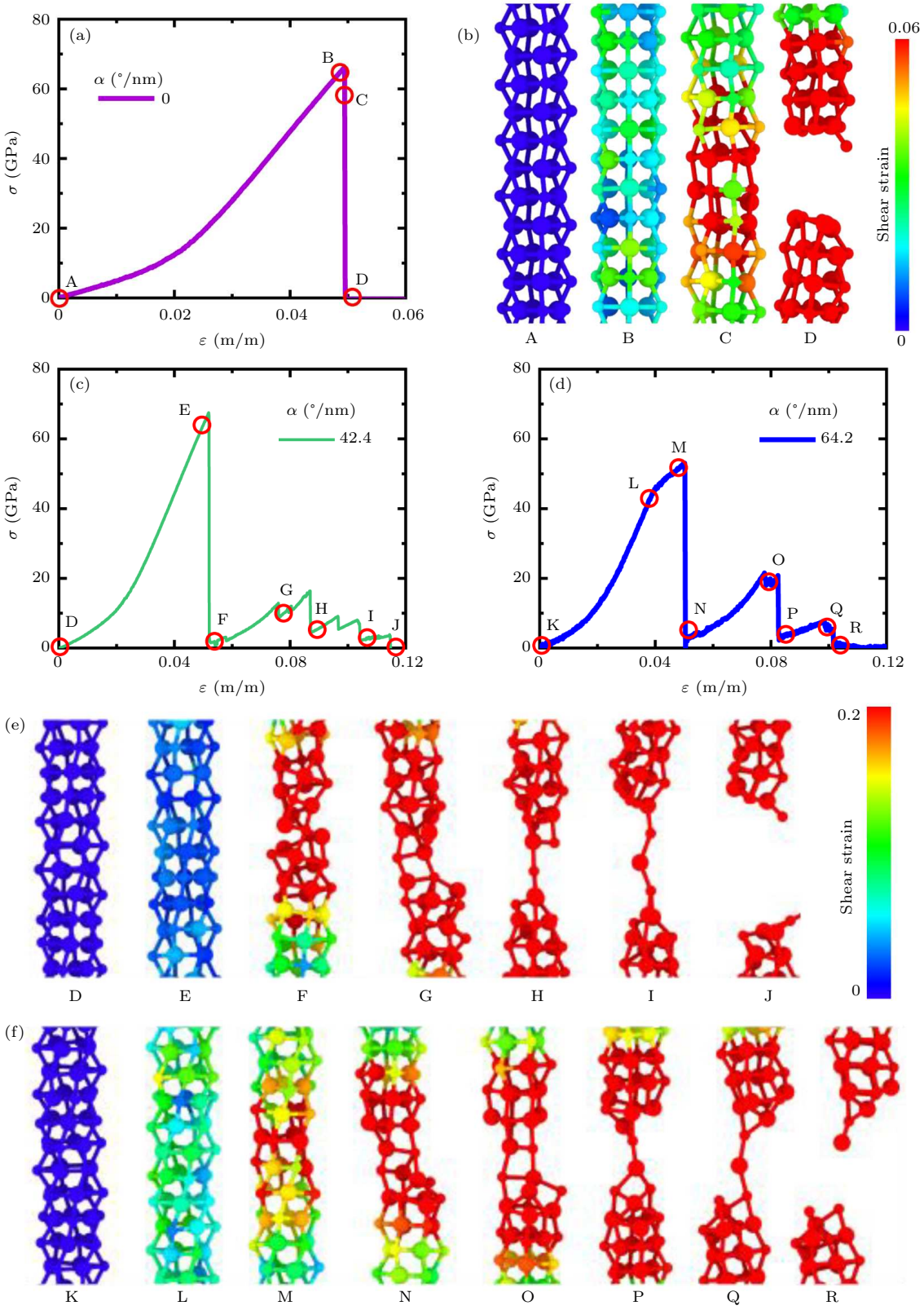


Fig. 6. Representative snapshots of molecular configurations of Mo_6S_6 NWs with $\alpha = 0$ °/nm, 42.4 °/nm, and 64.2 °/nm indicative of two distinct failure patterns. For clarification, the atoms are rendered on the basis of the values of the shear strain.

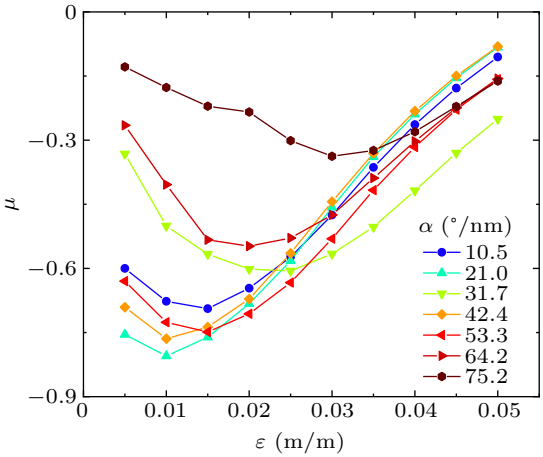


Fig. 7. The relations between the Poisson's ratio and applied strain during uniaxial tension of torsional Mo_6S_6 NW.

To further provide atomic insights into the auxetic property, the variations in the bond configurations with axial strain are investigated. Figure 8 shows the average bond distances (L_{Mo-S}) of two critical oriented Mo–S bonds that make angles of 0° and 90° to the axial direction of Mo_6S_6 NW subjected to different α as a function of axial strain. Subjected to global axial extension, the two critical oriented Mo–S bonds in Mo_6S_6 NW show distinct scenarios in the variations of L_{Mo-S} with axial strain. For the Mo–S bonds that make 0° to the axial direction of Mo_6S_6 NW, L_{Mo-S} is enlarged with increasing axial strain. However, the enlargement of L_{Mo-S} is nonlinearly increased but becomes less significant with the augment of axial strain. This indicates that the elongation of Mo_6S_6 NW is locally dominated not only by the bond stretching but also by angular deformation. With regard to the Mo–S bonds that make 0° to the lateral cross-section of NW, they are lengthened when Mo_6S_6 NW is axially stretched. Such lengthening of the laterally-oriented Mo–S bonds is the origin of the auxetic behavior, namely, negative Poisson's ratio. However, there is an unusual strain-dependent lengthening of the laterally-oriented Mo–S bonds. For example, there is a flipped behavior of L_{Mo-S} of all twisted Mo_6S_6 NW at critical axial strains. Below which, L_{Mo-S} is monotonically elongated, whereas over which, L_{Mo-S} is monotonically shortened with increasing axial strain. Such crossover of L_{Mo-S} explains the flipped behavior in the Poisson's ratio-strain curves as Mo_6S_6 NW is axially stretched.

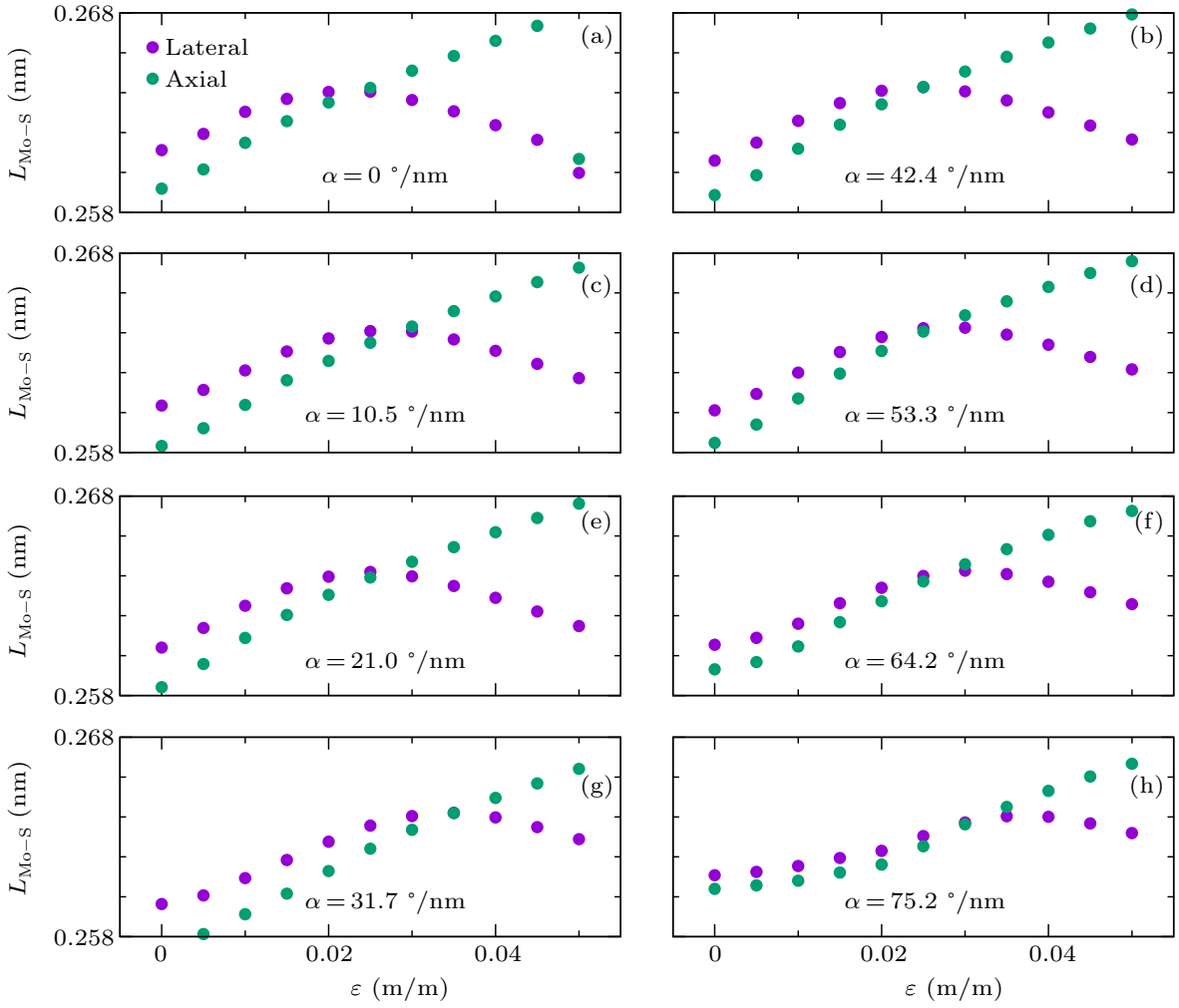


Fig. 8. (a)–(h) Average bond length of Mo–S as a function of tension strains, respectively. Here, two critical oriented Mo–S bonds that make 0° and 90° to the wire axial direction are investigated for bond lengths, named axial and lateral, respectively.

4. Conclusion and perspectives

The role of twist operation on the mechanical properties of Mo_6S_6 NW is explored using the first-principles-based ReaxFF MD simulations. The lattice constant and structural stability of Mo_6S_6 NW subjected to different torsional angles is studied. The torsional and bending stiffnesses of Mo_6S_6 NW are calculated to be around 3.26×10^{-4} kcal/mol/nm/deg^2 and 1.81 kcal/mol, respectively, indicating its higher torsional and bending flexibility than other 1D materials such as single-walled CNT, Si NWs and 2D materials graphene, single-layer black phosphorus, single-layer MoS_2. The tensile mechanical characteristics of twisted Mo_6S_6 NW are comprehensively investigated. It is calculated that the tensile strength of Mo_6S_6 NW can be enhanced or reduced, relying on the α. Mo_6S_6 NW with intermediate α shows the highest tensile strength. Moreover, all twisted Mo_6S_6 NWs show auxetic behavior, and the value of negative Poisson's ratios can be tuned by the α and axial strain. The unique strain-dependent lengthening of the bonds that make zero angles to the NW cross-section is the origin of the negative and U type Poisson's ratio with strain in Mo_6S_6 NW.

Acknowledgments

Y. Yu, Z. Xu, W. He, S. Fang, and T. Fu from Information and Network Center of Xiamen University for the help with the high-performance computer. Project supported by the National Natural Science Foundation of China (Grant Nos. 12172314, 11772278, 12002350, and 11904300), the Jiangxi Provincial Outstanding Young Talents Program (Grant No. 20192BCBL23029), the Fundamental Research Funds for the Central Universities of Xiamen University (Grant Nos. 20720210025 and 20720220023), and the "111" Project (Grant No. B16029).

References

[1] Lee C, Wei X, Kysar Jeffrey W and Hone J 2008 *Science* **321** 385
[2] Balandin A A 2011 *Nat. Mater.* **10** 569
[3] Popov I, Yang T, Berber S, Seifert G and Tománek D 2007 *Phys. Rev. Lett.* **99** 085503
[4] Shao Y, Meng F S, Li J H and Zhao X 2019 *Acta Phys. Sin.* **68** 216201 (in Chinese)
[5] Wang P, Zhang N C, Jiang C L, Liu F S, Liu Z T and Liu Q J 2020 *Chin. Phys. B* **29** 076201
[6] Zhou Y, Zhang X and Hu M 2017 *Nano Lett.* **17** 1269
[7] Liang T, Xu K, Han M, Yao Y, Zhang Z, Zeng X, Xu J and Wu J 2022 *Mater. Today Phys.* **25** 100705
[8] Liu M, Artyukhov V I, Lee H, Xu F and Yakobson B I 2013 *ACS Nano* **7** 10075
[9] Gao E, Li R and Baughman R H 2020 *ACS Nano* **14** 17071
[10] Gao E, Yuan X, Nielsen S O and Baughman R H 2022 *Phys. Rev. Appl.* **18** 014044
[11] Le D, Sun D, Lu W, Aminpour M, Wang C, Ma Q, Rahman T S and Bartels L 2013 *Surf. Sci.* **611** 1
[12] Huang W, Wang X, Ji X, Zhang Z and Jin C 2018 *Nano Res.* **11** 5849
[13] Xu K, Deng S, Liang T, Cao X, Han M, Zeng X, Zhang Z, Yang N and Wu J 2022 *Nanoscale* **14** 3078
[14] Kibsgaard J, Tuxen A, Levisen M, Lægsgaard E, Gemming S, Seifert G, Lauritsen J V and Besenbacher F 2008 *Nano Lett.* **8** 3928
[15] Vilfan I 2006 *Eur. Phys. J. B* **51** 277
[16] Lin J, Cretu O, Zhou W, Suenaga K, Prasai D, Bolotin K I, Cuong N T, Otani M, Okada S, Lupini A R, Idrobo J C, Caudel D, Burger A, Ghimire N J, Yan J, Mandrus D G, Pennycook S J and Pantelides S T 2014 *Nat. Nanotechnol.* **9** 436
[17] Çakır D, Durgun E, Gülseren O and Ciraci S 2006 *Phys. Rev. B* **74** 235433
[18] Liu X, Xu T, Wu X, Zhang Z, Yu J, Qiu H, Hong J H, Jin C H, Li J X, Wang X R, Sun L T and Guo W 2013 *Nat. Commun.* **4** 1776
[19] Souza D F, Rosa A L, Venezuela P, Padilha J E, Fazzio A and Pontes R B 2019 *Phys. Rev. B* **100** 235416
[20] Ying P, Zhang J, Zhou J, Liang Q and Zhong Z 2020 *Comput. Mater. Sci.* **179** 109691
[21] Murugan P, Kumar V, Kawazoe Y and Ota N 2007 *Nano Lett.* **7** 2214
[22] Popov I, Gemming S, Okano S, Ranjan N and Seifert G 2008 *Nano Lett.* **8** 4093
[23] Koskinen P 2016 *Phys. Rev. Appl.* **6** 034014
[24] Kibsgaard J 2008 *Atomic-scale investigation of* MoS_2*-based hydrotreating model catalysts* (Ph.D. Thesis) (Aarhus: University of Aarhus)
[25] Plimpton S 1995 *J. Comput. Phys.* **117** 1
[26] Large-scale Atomic/Molecular Massively Parallel Simulator
[27] Chenoweth K, van Duin A C T and Goddard W A 2008 *J. Phys. Chem. A* **112** 1040
[28] Ostadhossein A, Rahnamoun A, Wang Y, Zhao P, Zhang S, Crespi V H and van Duin A C T 2017 *J. Phys. Chem. Lett.* **8** 631
[29] Farahani H, Rajabpour A, Khanaki M and Reyhani A 2018 *Comput. Mater. Sci.* **142** 1
[30] Lin C, Chen X and Zou X 2019 *ACS Appl. Mater. Interfaces* **11** 25547
[31] Srivastava D, Wei C and Cho K 2003 *Appl. Mech. Rev.* **56** 215
[32] Vijayaraghavan V, Dethan J F N and Gao L 2018 *Sci. China Phys. Mech.* **62** 34611
[33] Jing Y and Meng Q 2010 *Physica B* **405** 2413
[34] Pan D 2015 *Chin. Sci. Bull.* **60** 764 (in Chinese)
[35] Bertolazzi S, Brivio J and Kis A 2011 *ACS Nano* **5** 9703
[36] Nicklow R, Wakabayashi N and Smith H G 1972 *Phys. Rev. B* **5** 4951
[37] Lu Q, Arroyo M and Huang R 2009 *J. Phys. D: Appl. Phys.* **42** 102002
[38] Torres-Dias A C, Cerqueira T F T, Cui W, Marques M A L, Botti S, Machon D, Hartmann M A, Sun Y, Dunstan D J and San-Miguel A 2017 *Carbon* **123** 145
[39] Wu J, Nie G, Xu J, He J, Xu Q and Zhang Z 2015 *Phys. Chem. Chem. Phys.* **17** 32425
[40] Gao E, Guo Y, Wang Z, Nielsen S O and Baughman R H 2022 *Matter* **5** 1192
[41] Li C and Chou T W 2003 *Int. J. Solids Struct.* **40** 2487
[42] Candido L M, Miotto L N, Fais L M G, Cesar P F and Pinelli L A P 2018 *Oper. Dent.* **43** E119
[43] Suryavanshi A P, Yu M F, Wen J, Tang C and Bando Y 2004 *Appl. Phys. Lett.* **84** 2527
[44] Kaplan-Ashiri I and Tenne R 2007 *J. Clust. Sci.* **18** 549
[45] Xiong Q L, Zhang J, Xiao C and Li Z H 2017 *Phys. Chem. Chem. Phys.* **19** 19948
[46] Lorenz T, Teich D, Joswig J O and Seifert G 2012 *J. Phys. Chem. C* **116** 11714
[47] Wu J Y, Nagao S, He J Y and Zhang Z L 2011 *Nano Lett.* **11** 5264
[48] Wu J, Cao P, Zhang Z, Ning F, Zheng S S, He J and Zhang Z 2018 *Nano Lett.* **18** 1543
[49] Wu J, He J, Ariza P, Ortiz M and Zhang Z 2020 *Int. J. Fract.* **223** 39
[50] Yang L, Liu J, Lin Y, Xu K, Cao X, Zhang Z and Wu J 2021 *Chem. Mater.* **33** 8758
[51] Wu J, Nagao S, He J and Zhang Z 2013 *Small* **9** 3561
[52] Wu J, He J, Odegard G M, Nagao S, Zheng Q and Zhang Z 2013 *J. Am. Chem. Soc.* **135** 13775
[53] Wu J, Zhao H, Liu J, Zhang Z, Ning F and Liu Y 2018 *Carbon* **133** 335
[54] Wu J, Shi Q, Zhang Z, Wu H H, Wang C, Ning F, Xiao S, He J and Zhang Z 2018 *Nanoscale* **10** 15641
[55] Jiang J W and Park H S 2014 *Nat. Commun.* **5** 4727
[56] Qian S, Sheng X, Zhou Y, Yan X, Chen Y, Huang Y, Huang X, Feng E and Huang W 2018 *J. Phys. Chem. C* **122** 7959
[57] Jin W, Sun W, Kuang X, Lu C and Kou L 2020 *J. Phys. Chem. Lett.* **11** 9643
[58] Wu J Y, He J Y and Zhang Z L 2013 *Comput. Mater. Sci.* **80** 15
[59] Lin Y, Xu K, Cao X, Zhang Z and Wu J 2021 *Mech. Mater.* **162** 104035